ELSEVIER

Contents lists available at ScienceDirect

Journal of Magnetism and Magnetic Materials

journal homepage: www.elsevier.com/locate/jmmm





Review of voltage-controlled magnetic anisotropy and magnetic insulator[★]

Bingqian Dai, Malcolm Jackson, Yang Cheng, Haoran He, Qingyuan Shu, Hanshen Huang, Lixuan Tai, Kang Wang *

Department of Electrical and Computer Engineering, Physics and Astronomy, and Material Science and Engineering, University of California, Los Angeles, CA 90095, United States

ABSTRACT

This Festschrift is dedicated to Chia-Ling Chien on the occasion of his eightieth birthday. Prof. Chien is one of the pioneering physicists in the field of spintronics with groundbreaking achievements in giant magnetoresistance, proximity effects in superconductor/ferromagnet multilayers, exchange bias, spin-transfer torque effect, voltage-controlled spin mechanisms, spin-caloritronics and so on. We will focus and give a brief review on the two aspects, the voltage-controlled magnetic anisotropy (VCMA), the magnetic insulator (MI), and related works.

1. Introduction

Electric field control of magnetism enhances the energy efficiency of spintronic devices. It goes beyond conventional nonvolatile spintronic applications by making them more energy efficient than traditional semiconductor solutions for logic and computation. Insulator-based spintronic devices are another promising candidate for next-generation memory technology. Introducing an insulator as the magnetic layer gives smaller Gilbert damping and reduces energy consumption. This paper will review recent progress on voltage-controlled magnetic anisotropy (VCMA) and magnetic insulators.

2. Voltage-controlled magnetic anisotropy

2.1. Mechanism

The exact microscopic origin of the VCMA effect remains unclear, and many experimental and theoretical research undertaken will continuously reveal the underlying mechanisms. The earlier studies show that the magnetic anisotropy field can change dramatically due to various chemical reactions, yet the underlying mechanism strongly depends on many factors such as the choice of material, the geometrical configuration, the crystal symmetry as well as experimental setup. Unfortunately, there is currently no clear explanation as to the exact mechanism by which the VCMA is induced for a given material. This is a major limitation that prevents the experimentalists from designing effective materials and interfaces with enhanced VCMA. In the

literature, there are many different concepts on the topic of voltage control of magnetism (VCM). We only mention here a few of the concepts while leaving our main discussion on the topic of the VCMA seen in ultrathin ferromagnetic heterostructures and directing the reader to more comprehensive reviews for further insight [1–3].

The first obvious source for the underlying mechanism of the VCM effect is the modification of charge carrier density due to the electric field. For this effect, the magnetic properties of a material should be coupled to the carrier density so that changes in carrier doping levels have a significant impact on the magnetic properties. However, for metals, it was initially thought this effect could be neglected due to the short screening length. It was soon realized that for ultrathin metal systems, the electric field does lead to a modulation of the carrier density and electron occupancy, which for 3d transition materials leads to a spin-dependent screening at the surface of the material, and in effect this can result in the modulation of the magnetocrystalline anisotropy energy (MAE) [1].

In most cases, the electric field's effect on the magneto-crystalline anisotropy (MCA) energy can be predicted by the theoretical first principle's electronic structure calculations [4]. These first principles studies indicate that to control the anisotropy effects, two basic mechanisms can be considered. These include the modulation of carrier density [5] or the orbital reconstruction effect [6], both of which hold similar consequences. These two different mechanisms lead to a VCMA, and yet fundamentally both effects can be explained by a modulation of the electronic band structure or through the spin–orbit coupling (SOC) induced magnetic anisotropy changes when placed under an electric

^{*} Corresponding author.

E-mail addresses: bdai@g.ucla.edu, wang@ee.ucla.edu (K. Wang).

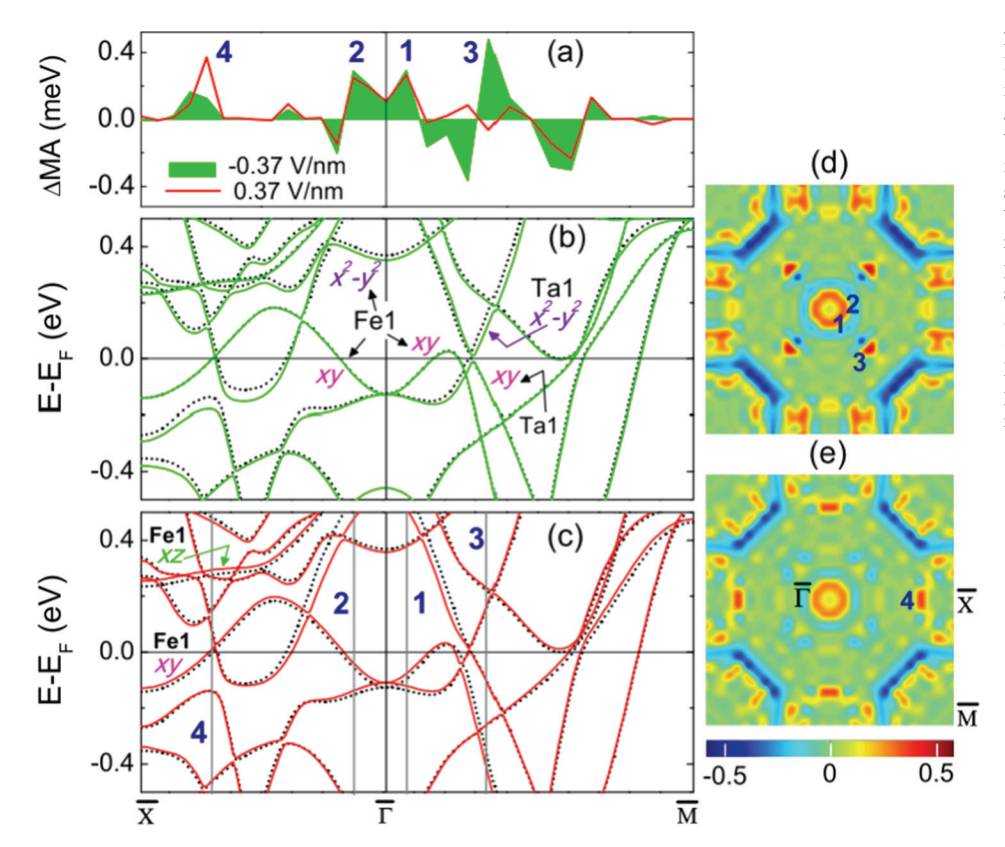


Fig. 1. MCA and electric field. (Reprint Ref. [13]) (Color online) Zero strain: (a) E-fieldinduced change in magnetic anisotropy (\Delta MA(k)) along high symmetry directions for $E_{I}=\pm0.37$ V/nm, where E_I is the electric field within the insulator. (b) and (c) Shift in zero-field minorityspin band structures (dotted curves) under -0.37 V/nm (solid green curves) and +0.37 V/nm (solid red curves) fields, respectively. The results are projected onto the dominant Fe and Ta d-orbital states. E-field-induced $\Delta MA(k)$ (in meV) in the 2D BZ for (d) $E_{I}\,=\,-0.37$ V/nm and (e) $E_{I}\,=\,$ +0.37 V/nm, respectively. The numbered vertical lines in (b) and (c) correspond to the numbered peaks in (a), (d), and (e), where the color scale represents the k-point resolved $\Delta MA(k)$.

field.

The concept of spin–orbit coupling (SOC) is a central property of ferromagnetism. SOC energy $H_{SOC} = \vartheta \mathbf{L} \bullet \mathbf{S}$ arises from the consideration of special relativity in the treatise of the coupling between the spin moment \mathbf{S} and the electron orbital moment \mathbf{L} , where ϑ is the SOC strength. The SOC interaction can lead to spin–lattice effects such as the MCA energy [7] and novel interface physics such as the Dzyaloshinskii-Moriya interaction [8] and the Rashba effect [9]. The MCA energy refers to the energy difference between the hard and easy axes of a magnetic material with $E_{ani} \approx E_{SOC}(Hard) - E_{SOC}(Easy)$ where the SOC energy can be theoretically treated using a second-order perturbation theory as developed in ref [10].

$$E_{SOC} = \vartheta^2 \sum_{o,u} \frac{\left| \left\langle o^m \mid L \bullet S \mid u^m \right\rangle \right|^2}{\varepsilon_u^m - \varepsilon_o^m} \tag{1}$$

where the superscript m denotes the minority spin states, o represents an occupied state and u represents an unoccupied state, and $\varepsilon_u^m - \varepsilon_o^m$ refers to the energy difference between any two occupied and unoccupied states.

For 3d transition metals (Fe, Cr, and alike), the crystal symmetries have a strong influence on the orbital momentum. As mentioned above, the orbital moment and atomic spin moment are strongly coupled through SOC; therefore, the energy of the system will be strongly dependent on the magnetization direction with respect to crystallographic directions. For 3d transition metals, the SOC is dominated by the d-orbital electrons. Due to a large energy difference between opposite spins the resulting SOC energies from spin mixing terms will be negligible, hence the equation above represents the SOC-induced MCA from the minority spins contribution. From Eq. (1) the modulation of the MCA can be attributed to a modulation of the electron states wave function via the numerator terms [11], or changes in the energy separation of the denominator. Peng et al. [12] present a comprehensive study of the magnetic anisotropy energy of different heavy metal caping materials in the CoFe/MgO/X multilayer structures. The study takes into account the

capping layer of these structures, composed of various 5d metals like Hf, Ta, Ir, Pt, and Pb, revealing the role heavy metals with a large SOC have on the perpendicular magnetic anisotropy (PMA). The results reveal large anisotropy values are predicted for the Ir, Pt, and Pb capping layers.

More recently, the importance of the VCMA at the FM/MgO interfaces has been theoretically investigated by various researchers. P. V. Ong et al. [13] provide an example of the change of energy separation in the denominator of Eq. (1) has on the magnetic anisotropy change in Ta/FeCo/MgO structures under different external electric field strengths (Fig. 1). Using the state tracking approach developed in [10] Eq. (1) can be used to identify the origin of the VCMA, which entails a full analysis of the modulation of both occupied and unoccupied energy bands near and around the Fermi level throughout the full Brillouin zone for each different electric field as seen in Fig. 1 (a).

In addition, S.Kwon et al. [14] recently show strain to be an important consideration in the electric field-induced magnetic behavior in CoFe/MgO/HM, where the theoretical first principles results works reveal the multilayer stacks with atomically thin HM capping layers, in combination with interfacial strain can induce colossal VCMA coefficients on the order of ~1000 fJ/Vm, which has been verified experimentally [15,16]. In essence, the strain effect can also be explained by the change of the band structure, via strain induced deformation potentials. In addition, first principles calculations reveal the atomically thin HM material may become magnetic under large strain [17]. Furthermore, the strain will also induce a change in the MgO dielectric constant, enhancing the density of screened charge at the FM/MgO interface. Ultimately, a linear dependence of the VCMA coefficient with the dielectric constant of the insulating material is shown below [13,14].

$$\xi = \frac{\Delta K_i}{\Delta E} = \frac{k \Delta \sigma_q}{\Delta E} = k \epsilon_0 \epsilon_{eff} \tag{2}$$

where the interfacial PMA change is represented as $\Delta K_i = k \Delta \sigma_q$, where k is a linear coefficient in the interfacial PMA per charge density

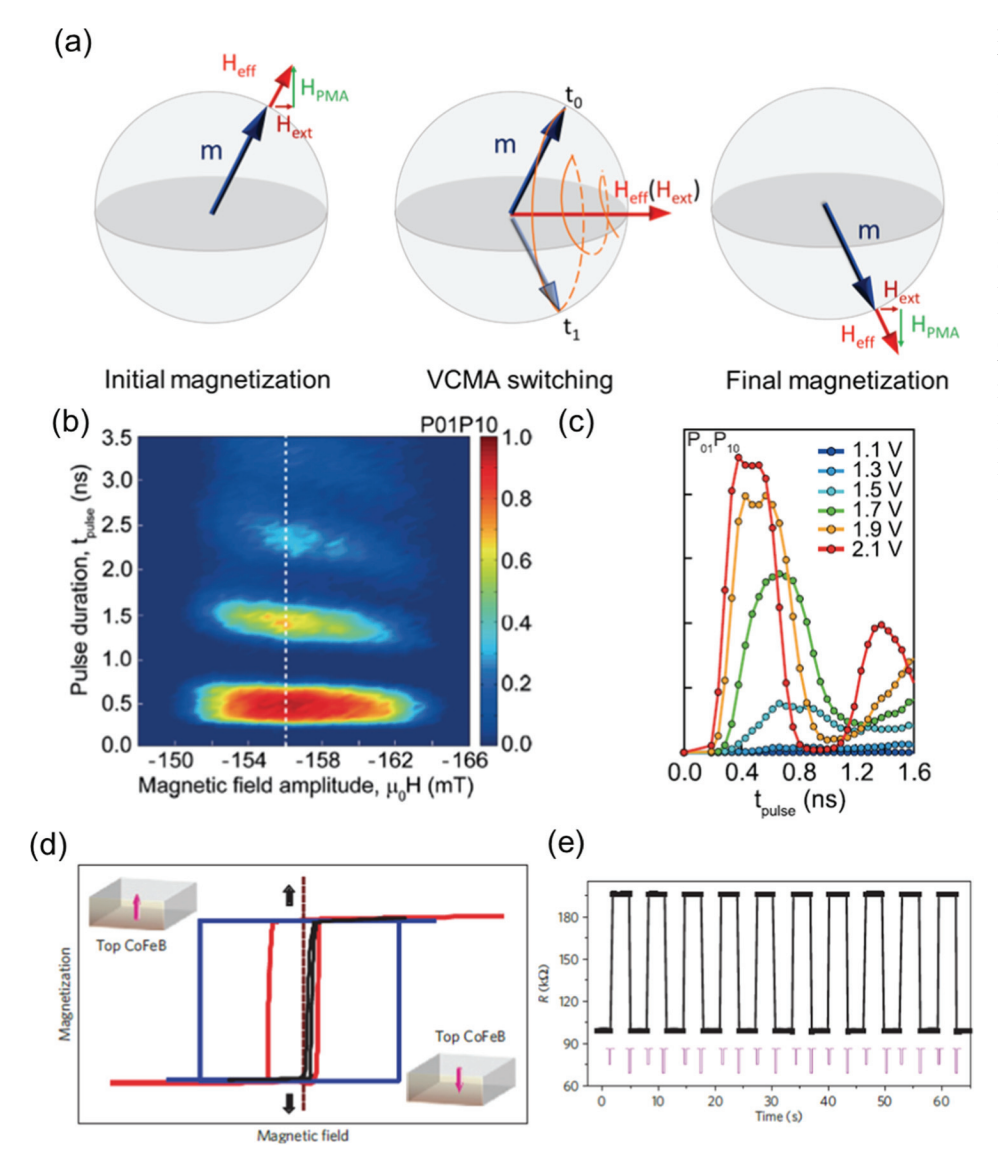


Fig. 2. VCMA switching. MTJ Switching by VCMA (a) Schematic of VCMA dynamic switching. (b) Switching probabilities of back and forth switching (P01P10) for 1.9 V voltage pulses as functions of pulse duration t_{pulse} and magnitude $\,$ of the external magnetic field. (c) P01P10, probabilities of switching from 0 to 1 and 1 to 0, respectively, as a function of the pulse width and amplitude. (d) Schematic diagram of the hysteresis loops of the top CoFeB layer, showing the unipolar switching process: magnetization down to up switching at small voltage (red) through STT with a greatly reduced energy barrier via VCMA; magnetization-up to down switching at large voltage (black) by another negative electric field. The reference loop with almost zero voltage is shown in blue. (e) Unipolar switching of the MTJ by a series of negative pulses. (b) and (c) are from Ref. [20], (d) and (e) are from Ref. [22].

change at the ferromagnetic/insulator interface, $\sigma_q = \frac{\epsilon_0 \epsilon_{eff} V}{d} = \epsilon_0 \epsilon_{eff} E$ is the induced surface charge density with ϵ_0 being the permittivity of free space, and ϵ_{eff} is the effective dielectric constant of the tunnel barrier, and ΔE is the change in the electric field at the FM/MgO interface. Therefore, if the tunnel barrier dielectric constant is increased, the VCMA coefficient can also be increased, while other previous reports show the strain to play an important role of the dielectric constant of MgO based junctions [13].

It is important to note that the theoretical calculations of FeCo/MgO assume that these materials have a perfect interface and crystal orientation. However, these calculations are not always representative of experiments due to the various defects present in the practical materials. For instance, most often sputter-deposited materials are used, and the polycrystalline state of these materials can vary, therefore direct comparisons of the theory and experiments could be challenging.

2.2. Voltage-controlled magnetic tunnel junction

The use of VCMA is a promising avenue for the next generation of MRAM technology, in spite of that the origin of VCMA will continue to be investigated. Unlike conventional current-controlled switching mechanisms such as spin-transfer torque (STT) and spin-orbit torque (SOT), voltage control can significantly reduce switching voltage and

current, and thus power consumption. Fig. 2(a) shows the schematic of the dynamic VCMA switching. The applied voltage eliminates the PMA and results in magnetic moment precession along the external field direction. After precession of half period, voltage is turned off so that PMA recovers and the moment will be stable in the opposite direction [18-20]. The typical switching behavior is shown in Fig. 2 (b) and (c) [20]. A clear periodic behavior is observed, indicating the nature of precession. The speed of such switching is sub-ns limited by the ferromagnetic resonance frequency. And the power consumption can be scaled down to sub fJ, depending on the VCMA coefficient and the size of device, which is more than one order of magnitude better than currentbased (STT, SOT) switching technology. The high switching voltage shown in Fig. 2 (c) is due to the low VCMA coefficient (~32 fJ/Vm) and can be solved by replacing the high VCMA stack. Besides the application in MRAM, the VCMA device can also be used as a true random number generator [21] and stochastic computing since making the moment inplane via VCMA can have an equal probability of being 1 or 0 by removing the applied voltage.

However, such dynamic nondeterministic VCMA switching requires the precise control of pulse amplitude and width, which brings great challenges in device uniformity and circuit design for the array-level application. The deterministic voltage-based switching mechanism is desired, which brings the ideas about hybrid writing mechanism: VCMA

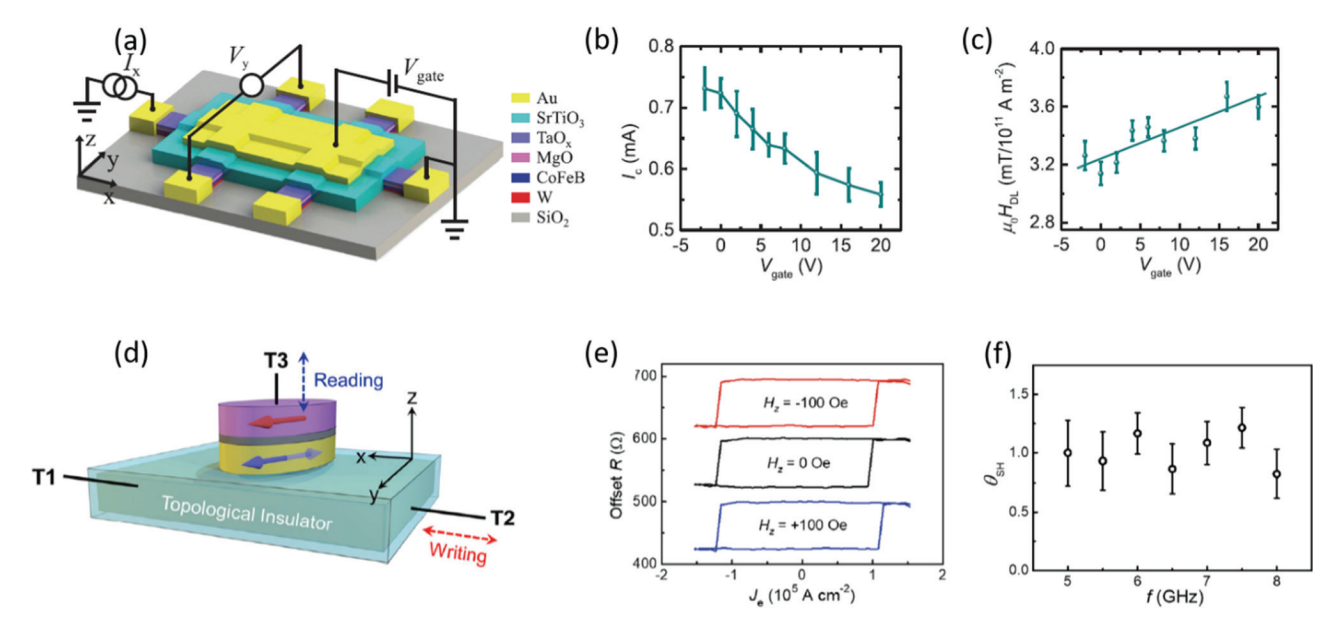


Fig. 3. Combining VCMA and SOT in MTJ. Switching by SOT (a) a Hall bar device for VCMA-SOT characterization; (b) critical current for SOT switching under different gate voltage [25]; (c) damping-like torque effective field extracted from the 2nd harmonic measurement; (d) a TI-MTJ device architecture; (e) field-free SOT switching of the in-plane MTJ; (f) spin Hall angle extracted from the ST-FMR measurement of the TI These numbers are considerably larger than heavy metals [28].

combined STT and VCMA combined SOT. Fig. 2 (d) shows the schematic of unipolar switching [22], achieved by VCMA combined STT. With the large voltage, the strong VCMA effect changes the hysteresis loop from the blue curve to the black curve, where only the magnetization down state is stable due to the external magnetic field. With the small voltage (red curve), though both magnetization up and down states are stable in the energy perspective, STT favors the up state and can achieve deterministic switching. Fig. 2 (e) [22] shows the reliable unipolar switching of the magnetic tunnel junction (MTJ) by a series of pulses. The switching speed is limited because of the high resistance-area product (RA) and thus low current density [22,23]. By reducing the RA, such switching can be achieved in a few ns [24]. However, the energy consumption increases and the benefits of voltage-based writing is somewhat compromised. Here we see the combining of VCMA and STT: in VCMA device, a high RA is essential to reduce the power consumption, while in STT device, a low RA can reduce the power consumption and improve the switching speed. The conflict originates from the shared channel of using both voltage and current in writing.

On the other hand, VCMA combined SOT does not have such an issue because the two mechanisms can be controlled independently, as will be discussed next.

2.3. Voltage-controlled SOT

The combination of VCMA and SOT establishes a synergetic relationship between the two mechanisms as shown in Fig. 3(a). For this combined VC-SOT structure, VCMA offers a reduced energy barrier during the writing operation that could enhance the energy efficiency of SOT switching. It is manifested in the reduction of critical SOT current by 23 % as shown in Fig. 3(b). Meanwhile, an enhancement of damping-like torque under the applied voltage is also observed 3(c), potentially due to the interfacial Rashba effect, spin mixing conductance, and the change of magnetic anisotropy, resulting from the alternation of interfacial electronic structure under the electric field as mentioned before [251].

On the other hand, SOT makes up the non-deterministic switching issue of VCMA. Since both effects for a perpendicular anisotropy structure need, in principle, an in-plane bias field to complete the deterministic switching process; integrating an embedded magnet into the MTJ devices [70] does not overcomplicate the device design and

switching behavior. Moreover, in contrast to combining STT with VCMA, which leads to the dilemma discussed above, the freedom to control SOT and VCMA independently provides more tuning knobs for device and/or material design. For instance, it has been experimentally discovered that topological insulators (TI) possess giant spin Hall angle, which could be orders of magnitude larger than that of the conventional heavy metals, owing to the spin-momentum locking of the surface Dirac electrons [27]. This spin-momentum locking provides a route to improve the SOT switching efficiency by incorporating TI into the MRAM technologies 3(d). A major step has been taken to demonstrate the compatibility of TI and MTJ devices [28]. In their work, as shown in Fig. 3(e), an ultralow switching current density of $1.2 \times 10^5 \, \mathrm{Acm}^{-2}$ has been achieved on high-quality in-plane MTJ with a 102 % TMR. Fig. 3(f) shows the measured spin Hall angle extracted from the ST-FMR measurement, which is considerably larger than that of heavy metal systems.

Aside from improving SOT and VCMA independently, a systematic study of combining the two effects has already taken place [26]. Applying a CMOS-compatible gate voltage of 1 V, the researchers achieved a 25 % write current reduction at 400 ps switching speed using 80 nm MTJ devices. Meanwhile, the endurance test has been performed under 1 V gate voltage and a current greater than the required switching current. There is no degradation after 10¹² cycles of operations, reflecting the robustness of the VCMA-SOT devices. However, challenges remain. One challenge comes from the gate selectivity of the MRAM devices because it requires a high VCMA coefficient to distinguish the MTJ to be switched from the rest. In short, finding material stacks that possess high VCMA, along with high TMR and high spin Hall angle simultaneously is essential for realizing a VCMA-SOT based MRAM technology that offers fast speed, high energy efficiency, and non-volatility.

3. Magnetic insulator

3.1. SOT

Insulator-based spintronic devices are promising candidates for the next generation memory technology as the introduction of an insulator as the magnetic layer gives smaller Gilbert damping and reduces energy consumption. Heavy metal/magnetic insulator heterostructure is explored with heavy metal ranging from Pt [29] to W [30], where the

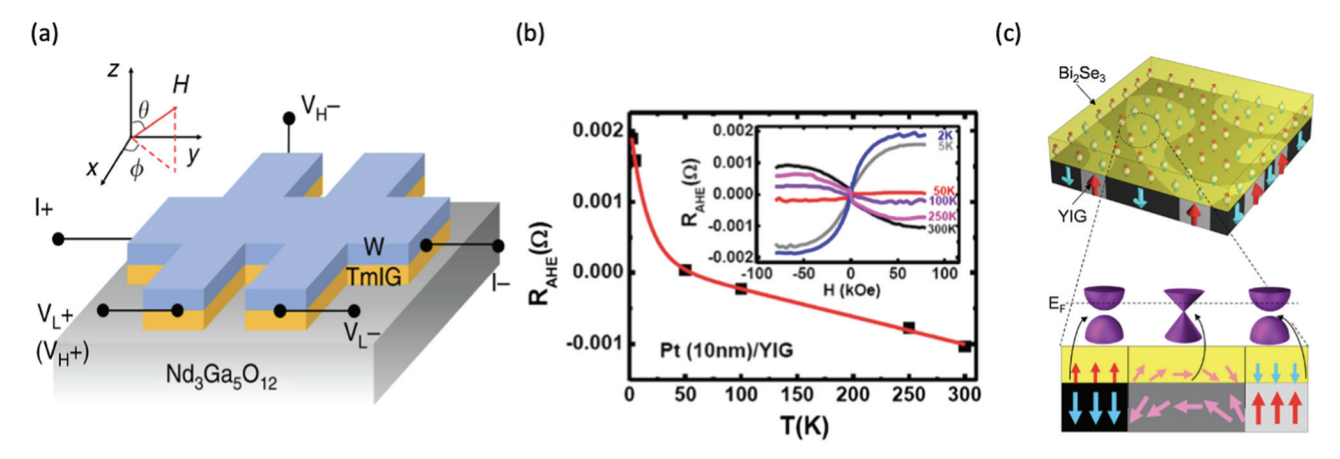


Fig. 4. (a) Transport measurement for SOT characterization in magnetic insulator TmIG. (b) Anomalous Hall resistance induced by magnetic proximity effect in Pt/YIG heterostructure. (c) Time-reversal symmetry breaking by magnetic proximity effect in TI/YIG heterostructure. (b) is from Ref. [36], (c) is from Ref. [39].

heavy metal layers can act as a spin current source due to the Spin Hall effect or as a spin-current receiver due to Inverse Spin Hall effect.

Compared with heavy metal/magnetic metal heterostructures such as Ta/CoFeB and Ta/GdFeCo, heavy metal/magnetic insulator heterostructures showed an order larger SOT efficiency [29]. As mentioned in the previous section, TI possesses a giant spin Hall angle which could be orders of magnitude larger than conventional heavy metal. By substituting the heavy metal layer with TI, the energy consumption can be further reduced, and the magnetization switching efficiency can be further boosted. The magnetization switching using SOT within this full insulator heterostructure has been realized in multiple materials ranging from garnets such as BaFe₁₂O₁₉ [31] to van der Waals materials such as $Cr_2Ge_2Te_6$ [32].

Recently, the study of insulating materials for spintronic devices has been extended from ferromagnets to antiferromagnets with zero net magnetization and faster writing speed due to its THz spin dynamics. Unlike ferromagnetic insulators where PMA samples are favorable, antiferromagnetic insulators used for SOT switching study mostly possess two or more in-plane easy axis such as NiO [33] and Fe_2O_3 [34]. Although the dynamics of antiferromagnetic insulators is faster compared with their ferromagnetic counterpart, the switching current might be also larger, resulting in thermal artifacts in transverse magnetoresistance when an eight-terminal pattern is used for measurement [35].

The characterization of magnetization switching within magnetic insulators could be a bit challenging due to the insulating nature of magnetic insulators. The characterization can be achieved either by indirect transport measurement or direct optical measurement. As is shown in Fig. 4(a), in transport measurement, the magnetic order induced by the proximity effect in the heavy metal [30] or TI layer can be monitored through the anomalous Hall effect [31]. While in optical measurement, the magnetization information of magnetic insulators can be directly characterized by the magneto-optical Kerr effect [29].

3.2. Proximity effect

The study of the interaction between two layers is of great essence for understanding the spin transport phenomena and building novel spintronic devices. The magnetic proximity effect is one of the major phenomena in magnetic heterostructure due to the interfacial contact with magnetic material. Through transport measurement, magnetic induced magnetic order within Pt through magnetic proximity effect has been discovered [36]. As is shown in Fig. 4(b) [36], Pt/YIG heterostructure shows anomalous Hall signal through 2 K to 300 K, which is not observed in Cu/YIG or Pt/Si heterostructure. And the induced magnetic ordering is further confirmed by X-ray magnetic circular dichroism (XMCD) measurement [37]. The following research explored the

entanglement between magnetic proximity effect and thermal effects in several heavy metal/magnetic insulator heterostructures, which ultimately promotes the detection of intrinsic Spin Seebeck effect through Au/YIG heterostructure [38].

For TI mentioned above, the topological surface state prevents the spin-moment locked Dirac Fermions from backscattering. In TI/magnetic insulator heterostructure, the property of TI is modified by the magnetic proximity effect by introducing magnetic order and breaking time-reversal symmetry, as is shown in Fig. 4(c) [39]. The breaking of time-reversal symmetry results in the observation of anomalous Hall effect in TI up to 130 K. The magnetic proximity effect between TI and the magnetic insulator is robust as the TI layer can be either molecular beam epitaxy grown [39] directly or wet transferred [40] on the magnetic insulator. Besides the ferromagnetic insulator, the antiferromagnetic insulator is also found to have a magnetic proximity effect in the adjacent TI layer [41], which could be due to the interfacial exchange interaction [42]. The study of the magnetic proximity effect in TI/magnetic insulator heterostructure paves the way toward high-temperature TI-based spintronic devices.

The study of the magnetic proximity effect has also been extended to van der Waals magnetic insulators after the discovery of two-dimensional magnets [43]. The atomic thickness and sharp interface make two-dimensional magnets a promising platform for studying the magnetic proximity effect. Recently, the magnetic proximity effect has been observed in nonmagnetic material/magnetic insulator heterostructure WSe $_2$ /CrI $_3$ [44]. The induced magnetic order within WSe $_2$ can be controlled by controlling the magnetic order of CrI $_3$ with an external field

3.3. Skyrmion

Magnetic skyrmions are topologically robust nanoscale spin textures that can be manipulated with low current densities and may be used as information carriers in future spintronic devices. Substantial efforts have focused on exploring room-temperature skyrmions in ferromagnet/heavy-metal systems. Previous works on such material systems demonstrated major advances, including room temperature spin-orbit torque creation and manipulation of skyrmions [45], room temperature skyrmion shift memory devices [46] and zero field stabilization of skyrmions by the antiferromagnetic order [47]. However, these metallic-based systems suffer from ohmic losses and, therefore, high energy dissipation. Magnetic insulators could provide a more energy-efficient skyrmionic platform due to their low damping and absence of Joule heating loss. A bilayer heterostructure composed of a magnetic insulating thulium iron garnet (Tm₃Fe₅O₁₂ or TmIG) thin film in contact with a platinum (Pt) film has been probed by the topological Hall effect (THE) to be the host of skyrmions [48]. Skyrmions are

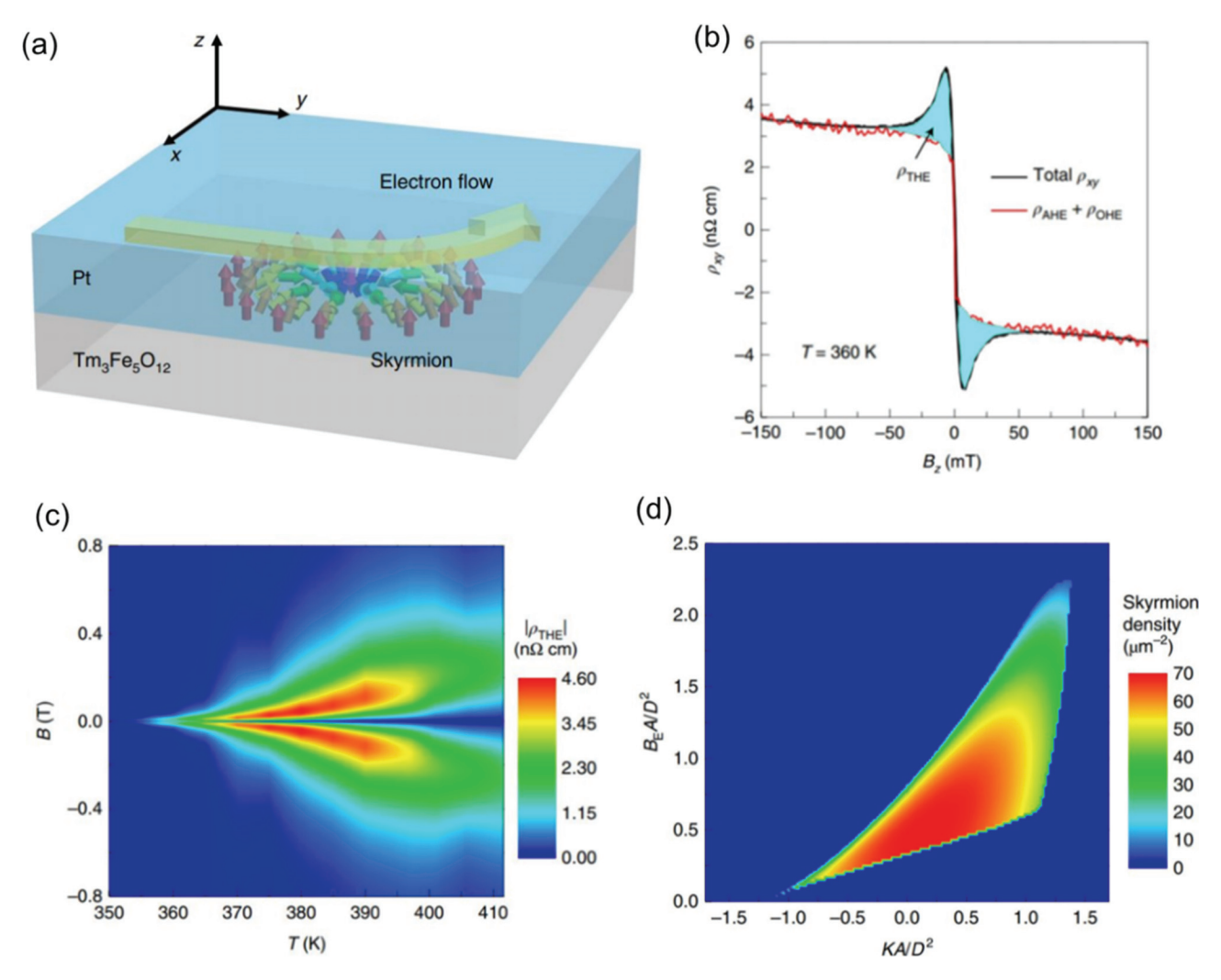


Fig. 5. Topological Hall effect (THE) in TmIG/Pt heterostructure. (Reprint Ref. [48]) (a) Schematic of the THE in the TmIG/Pt. The current in the Pt layer goes through in the presence of an emergent perpendicular magnetic field generated by the skyrmion in the TmIG and gives rise to the transverse Hall current. (b) Hall resistivity (black curve) as a function of an out-of-plane magnetic field at T = 360 K. The red curve shows the contribution of the AHE and the OHE. The light blue region indicates the contribution of THE. (c) Skyrmion phase diagram from the THE as a function of temperature T and external field Bz. The color bar indicates the value of the measured THE resistivity. Interpolation between experimentally measured data points is applied. (d) Theoretical skyrmion density diagram as a function of the normalized anisotropy energy (KA/D²) and the Zeeman energy (B_EA/D^2). All data are from the TmIG (3.2 nm)/Pt (4 nm) bilayer.

stabilized in this material by the interfacial DMI, which stems from strong spin-orbit coupling and a broken inversion symmetry at the TmIG/Pt interface. The exchange coupling between the skyrmions formed in TmIG and the finite spin polarization at the bottom Pt layer results in the THE (Fig. 5a). As will be discussed later, the origin and exact identification of THE remains to be further ascertained.

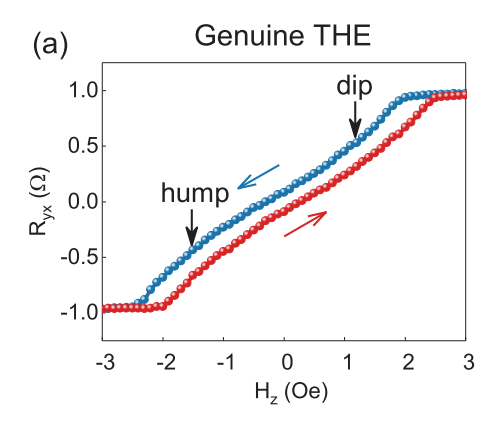
Exchange coupling between TmIG and Pt makes the conducting electrons spin-polarized, which results in the anomalous Hall effect (AHE) and spin Hall magnetoresistance (SMR) at and above room temperature in a patterned Hall bar device [49–51]. Assuming a smooth spin texture, the generic expression for anti-symmetric Hall resistivity (ρ_{xy}) can be obtained based on symmetry grounds.

$$\rho_{xy} = \rho_o B_z + \rho_A m_z + \frac{\rho_T}{4\pi} \iint d^2 r m \cdot \left(\frac{\partial m}{\partial x} \times \frac{\partial m}{\partial y} \right)$$
 (3)

where ρ_0 is the ordinary Hall effect (OHE) coefficient, ρ_A is the saturation AHE resistivity, m_z is the average z component of the magnetization unit vector in the Hall contact area, and the third term is the THE contribution (ρ_{THE}). In the THE term, ρ_T is the THE coefficient, and the integral counts how many times m(r)=m(x,y) wraps a unit sphere, which is the skyrmion topological number in real space. A

typical sharp hysteresis loop of ρ_{xy} is observed as a function of the out-of-plane external field (Bz) for the TmIG (3.2 nm)/Pt (4 nm) bilayer at 360 K, where the step function at low fields is due to the AHE, and the linear background with a negative slope at large fields arises from the OHE. Above 360 K, an unusual ρ_{xy} dip (or negative peak) at low positive fields and a peak at low negative fields emerge and gradually disappear at large fields, as shown in Fig. 5b. The overshoots in these out-of-plane hysteresis loops are identified as the THE due to the presence of magnetic skyrmions.

For practical purposes, skyrmions should be stable against external perturbations. The skyrmion phase diagram as a function of temperature and external field is experimentally obtained (Fig. 5c). The result shows that skyrmions are stable against thermal fluctuations up to 410 K under an external magnetic field of 0.4 T. By performing analytical and micromagnetic simulation, the experimental observations are confirmed to be consistent with calculations (Fig. 5d), and the prediction of [52]. Therefore, the temperature and external field dependencies of THE agree with the theoretical expectations, confirming the existence of magnetic skyrmions in TmIG/Pt. The discovery of skyrmions in a simple magnetic insulator/heavy metal bilayer heterostructure like TmIG/Pt at room temperature and above may benefit the development of practical



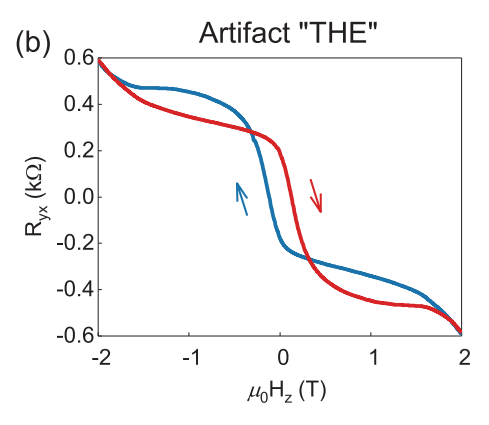


Fig. 6. Comparison of genuine THE and artifact THE. (Reprint Ref. [69]) (a) The skyrmion-induced genuine THE with AHE in the Ta(5)/CoFeB(0.9)/Ir(0.03–0.15)/MgO(2)/Al2O3(5). The blue and red arrows indicate the direction of the field sweep, and the black arrows indicate the hump and dip caused by THE. The measurement is performed at room temperature. (b) Artifact "THE" with AHE, or two-component AHE in the 7 SL MnBi $_2$ Te $_4$ sample. The measurement is performed at 2 K.

low-power, skyrmion-based applications. Fig. 5 is reproduced from Ref. [48].

4. Perspective

To go beyond manipulating uni-axial effects such as VCMA, controlling chirality by the anti-symmetric exchange coupling known as Dzyaloshinskii-Moriya interaction (DMI) [53,54] would be intriguing. Chirality is an asymmetric structural property for which an object cannot be mapped onto its mirror image, giving rise to a handedness. In magnetic materials, inversion symmetry breaking can give rise to chirality through DMI. The Hamiltonian is defined for neighboring atomic spins $S_{i,j}$ as: $H_{DMI} = -D_{ij} \bullet (S_i \times S_j)$ [53,54], where D_{ij} denotes the DMI vector. Bulk DMI arises from limited bulk materials with inversion asymmetry [55]. Interfacial DMI (iDMI) [56] arises due to the asymmetry from interface of a heavy metal/thin-film ferromagnet [57] heterostructure with strong spin-orbit coupling. iDMI stabilizes chiral topological spin textures, e.g., skyrmion and domain wall [58]. The characteristics of skyrmions and domain walls depend intimately on the iDMI. For instance, the handedness of a skyrmion is determined by the sign of iDMI [59], and the topological stability and the minimum size of the skyrmion can be varied by orders of magnitude by the iDMI strength [60]. Therefore, insightful understanding and effective control of iDMI are crucial. Progress in controlling iDMI has been made for different stackings of various HM/FM heterostructures [56] and likewise by introducing ionic species such as oxygen and hydrogen via chemisorption [61]. However, these methods either can only be enabled by built-in material structure (static) [56] or are slow in time (in minute time scale) [61]. The effect of electric fields will give rise to a more convenient and practical way to control DMI. Thus, the use of the electric field or voltage would offer a more functional device platform that is vital for lowenergy and high-speed operations [62]. The voltage-controlled DMI originating from the Rashba effect has been reported in the heavy metal/ ferromagnet/insulator heterostructure [63] and might be able to resolve the two drawbacks mentioned above. But the atomic scale understanding of the electric field manipulation has been rarely studied. Therefore, insightful investigation of this emerging electric field or voltagecontrolled DMI (VCDMI) effect would provide new opportunities for exploring new physics and applications and would provide the opportunity to go beyond the traditional VCMA effect.

Stabilized by iDMI, chiral topological spin textures, e.g., skyrmion, still under intense research to date, and one of the most important signatures of chiral topological spin textures in transport is the topological Hall effect (THE), manifesting itself as non-monotonic anomalies in the Hall signal as discussed before [64]. As shown in Eq. (3), the presence of anomalous Hall effect (AHE), the two-component AHE, i.e., the coexistence of two AHE loops, may also give rise to a non-monotonic shape that is similar to genuine THE with AHE, making it difficult to distinguish between the two. [65–68].

Reproduced from Ref. [69], Fig. 6 shows an example of genuine THE with AHE (Fig. 6a) from a Ta(5)/CoFeB(0.9)/Ir(0.03–0.15)/MgO(2)/Al₂O₃(5) structure grown by magnetron sputtering, in which magnetic skyrmions are directly observed by magneto-optical Kerr effect (MOKE) microscopy (not presented here), and another example of artifact "THE" with AHE (Fig. 6b), or two-component AHE in a 7 SL MnBi₂Te₄ sample grown by MBE with a secondary phase MnTe₂ contributing to the extra AHE component [69]. Strikingly, genuine THE occurs in the transition region of the AHE, while in sharp contrast, the artifact "THE" occurs even well after the "AHE component" becomes fully saturated. In short, non-monotonic anomalies in the Hall resistivity alone cannot be used as sufficient evidence for chiral spin textures such as skyrmions. Magneto-transport cannot be used to ascertain the existence of skyrmion, and other techniques such as MOKE, X-ray, and Lorentz TEM may be used to complement the investigation.

Declaration of Competing Interest

The authors declare that they have no known competing financial interests or personal relationships that could have appeared to influence the work reported in this paper.

Data availability

Data will be made available on request.

Acknowledgment

The authors acknowledge the support from the National Science Foundation (NSF) Award No. 1411085, No. 1810163, No. 1935362, No. 1909416, No. 1810163, and No. 1611570; the Nanosystems Engineering Research Center for Translational Applications of Nanoscale Multiferroic Systems (TANMS); the Intel Corporation under Contract No. 52318957; and the Army Research Office Multidisciplinary University Research Initiative (MURI) under grant numbers W911NF16-1-0472 and W911NF-19-S-0008.

References

- [1] C. Song, B. Cui, F. Li, X. Zhou, F. Pan, Recent progress in voltage control of magnetism: materials, mechanisms, and performance, Prog. Mater Sci. 87 (2017) 22 92
- N. Takayuki, T. Yamamoto, S. Miwa, M. Tsujikawa, M. Shirai, S. Yuasa, Y. Suzuki, Recent progress in the voltage-controlled magnetic anisotropy effect and the challenges faced in developing voltage-torque MRAM, Micromachines 10, 5 (2019) 327.
- [3] R. Ramamoorthy, S. Manipatruni, Electric field control of magnetism, Proc. R. Soc. A: Math. Phys. Eng. Sci. 477 (2021) 2251.
- [4] P.V. Ong, N. Kioussis, P.K. Amiri, K.L. Wang, G.P. Carman, Strain control magnetocrystalline anisotropy of Ta/FeCo/MgO heterostructures, J. App. Phys. 117 (17) (2015), 17B518.

- [5] C.-G. Duan, J.P. Velev, R.F. Sabirianov, Z. Zhu, J. Chu, S.S. Jaswal, E.Y. Tsymbal, Surface magnetoelectric effect in ferromagnetic metal films, Phys. Rev. Lett. 101 (2008), 137201.
- [6] J. Zhang, P.V. Lukashev, S.S. Jaswal, E.Y. Tsymbal, Model of orbital populations for voltage-controlled magnetic anisotropy in transition-metal thin films, Phys. Rev. B 96 (2017), 014435.
- [7] P. Bruno, Tight-binding approach to the orbital magnetic moment and magnetocrystalline anisotropy of transition-metal monolayers, Phys. Rev. B 39 (1989) 865(R).
- [8] T. Moriya, Anisotropic superexchange interaction and weak ferromagnetism, Phys. Rev. 120 (1960) 91.
- [9] E.I. Rashba, V.I. Sheka, Fiz. Tverd. Tela Collected Papers (Leningrad), v.II (1959) 162–176.
- [10] D.-S. Wang, R. Wu, A.J. Freeman, First-principles theory of surface magnetocrystalline anisotropy and the diatomic-pair model, Phys. Rev. B 47 (1993) 14932
- [11] P.V. Ong, N. Kioussis, P.K. Amiri, K.L. Wang, Electric-field-driven magnetization switching and nonlinear magnetoelasticity in Au/FeCo/MgO heterostructures, Sci. Rep. 6 (2016) 29815.
- [12] S. Peng, W. Zhao, J. Qiao, L. Su, J. Zhou, H. Yang, Q. Zhang, Y. Zhang, C. Grezes, P. K. Amiri, K.l. Wang, Giant interfacial perpendicular magnetic anisotropy in MgO/Cofe/capping layer structures, Appl. Phys. Lett. 110, 7 (2017), 072403.
- [13] P.V. Ong, N. Kioussis, D. Odkhuu, P. Khalili Amiri, K.L. Wang, G. p., Carman Giant voltage modulation of magnetic anisotropy in strained heavy metal/magnet/ insulator heterostructures, Phys. Rev. B 92 (2015), 020407.
- [14] S. Kwon, P.V. Ong, Q. Sun, F. Mahfouzi, X. Li, K.L. Wang, Y. Kato, H. Yoda, P. K. Amiri, N. Kioussis, Colossal electric field control of magnetic anisotropy at ferromagnetic interfaces induced by iridium overlayer, Phys. Rev. B 99 (2019) 6.
- [15] Y. Ohsawa, et al., Ultra-high-efficiency writing in voltage-control spintronics memory (VOCSM): the most promising embedded memory for deep learning, IEEE J. Electron Devices Soc. 6 (2018) 1233–1238.
- [16] Y. Kato, et al., Giant voltage-controlled magnetic anisotropy effect in a crystallographically strained CoFe system, Appl. Phys Express 11 (5) (2018), 053007.
- [17] Q. Sun, F. Mahfouzi, J.P. Velev, E.Y. Tsymbal, N. Kioussis, Ferroelectric-driven tunable magnetism in ultrathin platinum films, Phys. Rev. Mater. 4 (2020), 124401.
- [18] Y. Shiota, et al., Induction of coherent magnetization switching in a few atomic layers of FeCo using voltage pulses, Nat. Mater. 11 (1) (2012) 39–43.
- [19] S. Kanai, et al., Electric field-induced magnetization reversal in a perpendicular-anisotropy CoFeB-MgO magnetic tunnel junction, Appl. Phys. Lett. 101 (12) (2012), 122403.
- [20] C. Grezes, et al., Ultra-low switching energy and scaling in electric-field-controlled nanoscale magnetic tunnel junctions with high resistance-area product, Appl. Phys. Lett. 108 (1) (2016), 012403.
- [21] J. Yang et al., A calibration-free in-memory true random number generator using voltage-controlled MRAM, in: ESSDERC 2021-IEEE 51st European Solid-State Device Research Conference (ESSDERC), IEEE, 2021.
- [22] W.-G. Wang, et al., Electric-field-assisted switching in magnetic tunnel junctions, Nat. Mater. 11 (1) (2012) 64–68.
- [23] W.G. Wang, C.L. Chien, Voltage-induced switching in magnetic tunnel junctions with perpendicular magnetic anisotropy, J. Phys. D Appl. Phys. 46 (7) (2013), 074004.
- [24] S. Kanai, et al., Magnetization switching in a CoFeB/MgO magnetic tunnel junction by combining spin-transfer torque and electric field-effect, Appl. Phys. Lett. 104 (21) (2014), 212406.
- [25] J. Xu, C.-L. Chien, Voltage-controlled spin-orbit torque switching in W/CoFeB/MgO, Appl. Phys. Lett. 118 (5) (2021), 052409.
- [26] Y.C. Wu, et al., Voltage-gate-assisted spin-orbit-torque magnetic random-access memory for high-density and low-power embedded applications, Phys. Rev. Appl 15 (6) (2021), 064015.
- [27] Y. Fan, et al., Electric-field control of spin-orbit torque in a magnetically doped topological insulator, Nat. Nanotechnol. 11 (4) (2016) 352–359.
- [28] H. Wu, et al., Magnetic memory driven by topological insulators, Nat. Commun. 12 (1) (2021) 1–7.
- [29] M. Montazeri, P. Upadhyaya, M.C. Onbasli, G. Yu, K.L. Wong, M. Lang, Y. Fan, X. Li, P.K. Amiri, R.N. Schwartz, C.A. Ross, K.L. Wang, Magneto-optical investigation of spin-orbit torques in metallic and insulating magnetic heterostructures, Nat. Comm. 6 (2015) 1–9.
- [30] Q. Shao, C. Tang, G. Yu, A. Navabi, H. Wu, C. He, J. Li, P. Upadhyaya, P. Zhang, S. A. Razavi, Q.L. He, Y. Liu, P. Yang, S.K. Kim, C. Zheng, Y. Liu, L. Pan, R.K. Lake, X. Han, Y. Tserkovnyak, J. Shi, K.L. Wang, Role of dimensional crossover on spin-orbit torque efficiency in magnetic insulator thin films, Nat. Comm. 9 (1) (2018) 1–7.
- [31] P. Li, J. Kally, S.S.L. Zhang, T. Pillsbury, J. Ding, G. Csaba, J. Ding, J.S. Jiang, Y. Liu, R. Sinclair, C. Bi, A. DeMann, G. Rimal, W. Zhang, S.B. Field, J. Tang, W. Wang, O.G. Heinonen, V. Novosad, A. Hoffmann, N. Smarth, M. Wu, Magnetization switching using topological surface states, Sci. Adv. 5 (8) (2019).
- [32] M. Mogi, K. Yasuda, R. Fujimura, R. Yoshimi, N. Ogawa, A. Tsukazaki, M. Kawamura, K.S. Takahashi, M. Kawasaki, Y. Tokura, Current-induced switching of proximity-induced ferromagnetic surface states in a topological insulator, Nat Comm. 12 (2021) 1404.
- [33] X.Z. Chen, R. Zarzuela, J. Zhang, C. Song, X.F. Zhou, G.Y. Shi, F. Li, H.A. Zhou, W. J. Jiang, F. Pan, Y. Tserkovnyak, Antidamping-torque-induced switching in biaxial antiferromagnetic insulators, Phys. Rev. Lett. 120 (20) (2018), 207204.

- [34] Y. Cheng, S. Yu, M. Zhu, J. Hwang, F. Yang, Electrical switching of tristate antiferromagnetic Néel order in α -Fe2O3 epitaxial films, Phys. Rev. Lett. 124 (2) (2020), 027202.
- [35] C.C. Chiang, S.Y. Huang, D. Qu, P.H. Wu, C.L. Chien, Absence of evidence of electrical switching of the antiferromagnetic Néel vector, Phys. Rev. Lett. 123 (22) (2019), 227203.
- [36] S.Y. Huang, X. Fan, D. Qu, Y.P. Chen, W.G. Wang, J. Wu, T.Y. Chen, J.Q. Xiao, C. L. Chien, Transport magnetic proximity effects in platinum, Phys. Rev. Lett. 109 (10) (2012).
- [37] Y.M. Lu, Y. Choi, C.M. Ortega, X.M. Cheng, J.W. Cai, S.Y. Huang, L. Sun, C. L. Chien, Pt magnetic polarization on Y3Fe5O12 and magnetotransport characteristics, Phys. Rev. Lett. 110 (14) (2013).
- [38] D. Qu, S.Y. Huang, J. Hu, R. Wu, C.L. Chien, Intrinsic spin seebeck effect in Au/YIG, Phys. Rev. Lett. 110 (6) (2013).
- [39] M. Lang, M. Montazeri, M.C. Onbasli, X. Kou, Y. Fan, P. Upadhyaya, K. Yao, F. Liu, Y. Jiang, W. Jiang, K.L. Wong, G. Yu, J. Tang, T. Nie, L. He, R.N. Schwartz, Y. Wang, C.A. Ross, K.L. Wang, Proximity induced high-temperature magnetic order in topological insulator ferrimagnetic insulator heterostructure, Nano Lett. 14 (6) (2014) 3459–3465.
- [40] X. Che, K. Murata, L. Pan, Q.L. He, G. Yu, Q. Shao, G. Yin, P. Deng, Y. Fan, B. Ma, X. Liang, B. Zhang, X. Han, L. Bi, Q.H. Yang, H. Zhang, K.L. Wang, Proximity-induced magnetic order in a transferred topological insulator thin film on a magnetic insulator, ACS Nano 12 (5) (2018) 5042–5050.
- [41] Y. Liu, X. Niu, R. Zhang, Q. Zhang, J. Teng, Y. Li, Magnetic proximity effect in an antiferromagnetic insulator/topological insulator heterostructure with sharp interface, Chin. Phys. Lett. 38 (5) (2021), 057303.
- [42] C.Y. Yang, L. Pan, A.J. Grutter, H. Wang, X. Che, Q.L. He, Y. Wu, D.A. Gilbert, P. Shafer, E. Arenholz, H. Wu, G. Yin, P. Deng, J.A. Borchers, W. Ratcliff, K. L. Wang, Termination switching of antiferromagnetic proximity effect in topological insulator, Sci. Adv. 6 (33) (2020) 8463–8475.
- [43] C. Gong, L. Li, Z. Li, H. Ji, A. Stern, Y. Xia, T. Cao, W. Bao, C. Wang, Y. Wang, Z. Q. Qiu, R.J. Cava, S.G. Louie, J. Xia, X. Zhang, Discovery of intrinsic ferromagnetism in two-dimensional van der Waals crystals, Nature 546 (7657) (2017) 265–269.
- [44] T. Liu, J. Kally, T. Pillsbury, C. Liu, H. Chang, J. Ding, Y. Cheng, M. Hilse, R. Engel-Herbert, A. Richardella, N. Samarth, M. Wu, Changes of magnetism in a magnetic insulator due to proximity to a topological insulator, Phys. Rev. Lett. 125 (1) (2020), 017204.
- [45] G. Yu, et al., Room-temperature creation and spin-orbit torque manipulation of skyrmions in thin films with engineered asymmetry, Nano Lett. 16 (3) (2016) 1981–1988.
- [46] G. Yu, et al., Room-temperature skyrmion shift device for memory application, Nano Lett. 17 (1) (2017) 261–268.
- [47] G. Yu, et al., Room-temperature skyrmions in an antiferromagnet-based heterostructure, Nano Lett. 18 (2) (2018) 980–986.
- [48] Q. Shao, et al., "Topological Hall effect at above room temperature in heterostructures composed of a magnetic insulator and a heavy metal, Nat. Electron. 2 (5) (2019) 182–186.
- [49] C. Tang, et al., Anomalous Hall hysteresis in Tm3Fe5O12/Pt with strain-induced perpendicular magnetic anisotropy, Phys. Rev. B 94 (14) (2016), 140403.
- [50] Y.-T. Chen, et al., Theory of spin Hall magnetoresistance, Phys. Rev. B 87 (14) (2013), 144411.
- [51] S.-Y. Huang, et al., Transport magnetic proximity effects in platinum, Phys. Rev. Lett. 109 (10) (2012), 107204.
- [52] S. Banerjee, et al., Enhanced stability of skyrmions in two-dimensional chiral magnets with Rashba spin-orbit coupling, Phys. Rev. X 4 (3) (2014), 031045.
- [53] I. Dzyaloshinsky, A thermodynamic theory of "weak" ferromagnetism of antiferromagnetics, J. Phys. Chem. Solids 4 (4) (1958) 241–255.
- [54] T. Moriya, Anisotropic superexchange interaction and weak ferromagnetism, Phys. Rev. 120 (1) (1960) 91.
- [55] X.Z. Yu, et al., Real-space observation of a two-dimensional skyrmion crystal, Nature 465 (7300) (2010) 901–904.
- [56] X. Ma, et al., Interfacial dzyaloshinskii-moriya interaction: Effect of 5 d band filling and correlation with spin mixing conductance, Phys. Rev. Lett. 120 (15) (2018), 157204.
- [57] A. Fert, P.M. Levy, Role of anisotropic exchange interactions in determining the properties of spin-glasses, Phys. Rev. Lett. 44 (23) (1980) 1538.
- [58] W. Jiang, et al., Blowing magnetic skyrmion bubbles, Science 349 (6245) (2015) 283–286.
- [59] S. Emori, et al., Current-driven dynamics of chiral ferromagnetic domain walls, Nat. Mater. 12 (7) (2013) 611–616.
- [60] N. Romming, et al., Field-dependent size and shape of single magnetic skyrmions, Phys. Rev. Lett. 114 (17) (2015), 177203.
- [61] G. Chen, et al., Large Dzyaloshinskii-Moriya interaction induced by chemisorbed oxygen on a ferromagnet surface, Sci. Adv. 6 (33) (2020), eaba4924.[62] X. Li, et al., Enhancement of voltage-controlled magnetic anisotropy through
- precise control of Mg insertion thickness at CoFeB| MgO interface, Appl. Phys. Lett. 110 (5) (2017), 052401.
- [63] T. Srivastava, et al., Large-voltage tuning of Dzyaloshinskii-Moriya interactions: a route toward dynamic control of skyrmion chirality, Nano Lett. 18 (8) (2018) 4871–4877.
- [64] P. Bruno, V.K. Dugaev, M. Taillefumier, Topological Hall effect and Berry phase in magnetic nanostructures, Phys. Rev. Lett. 93 (9) (2004), 096806.
- [65] A. Gerber, Interpretation of experimental evidence of the topological Hall effect, Phys. Rev. B 98 (21) (2018), 214440.

- [66] N. Liu, J. Teng, Y. Li, Two-component anomalous Hall effect in a magnetically doped topological insulator, Nat. Commun. 9 (2018) 1282.
- [67] K.M. Fijalkowski, et al., Coexistence of surface and bulk ferromagnetism mimics skyrmion Hall effect in a topological insulator, Phys. Rev. X 10 (1) (2020), 011012.
- [68] P. Chen, et al., Tailoring the hybrid anomalous Hall response in engineered magnetic topological insulator heterostructures, Nano Lett. 20 (3) (2020) 1731–1737.
- [69] L. Tai, et al., Distinguishing the Two-Component Anomalous Hall Effect from the Topological Hall Effect, ACS Nano (2022), https://doi.org/10.1021/ acspano 2c08155
- [70] Y.C. Wu, et al., Deterministic and Field-Free Voltage-Controlled MRAM for High Performance and Low Power Applications, 2020 IEEE Symposium on VLSI Technology (2020) 1–2, https://doi.org/10.1109/ VLSITechnology18217.2020.9265057.